ISSN 1392–1320 MATERIALS SCIENCE (MEDŽIAGOTYRA). Vol. XX, No. X. 2023

Synthesis of Phosphotungstic acid/S-doped g-C_3N_4 Photocatalyst and Its Photocatalytic Degradation of Organic Pollutants in Aqueous Solutions

Pengxi LI *, Zhonghong LIU, Bing YANG, Zhiyong JIANG, Jingjing YANG *

Environment and Quality Test Department, Chongqing Chemical Industry Vocational College, Chongqing, 401228, P. R. China

crossref http://dx.doi.org/10.5755/j02.ms.31053

Received 04 April 2022; accepted 16 May 2022

The S-doped g-C_3N_4 (SCN) was prepared by thermal condensation method using thiourea as a precursor, and then the phosphotungstic acid (PTA)/SCN composite photocatalytic material was prepared by reflux adsorption method. The photocatalytic degradation experiments of Rhodamine B showed that SCN20 had the highest photocatalytic degradation rate (74 %), which was 1.9 times and 3.5 times higher than that of PTA (39 %) and SCN (21 %), respectively. The photocatalytic degradation rate of SCN20 was increased by 5 times compared to that of SCN, indicating that the photocatalytic degradation performance of the composite material was significantly improved. The photocatalytic degradation mechanism study revealed that O_2^- was the main active species in the photocatalytic degradation of Rhodamine B, and the addition of PTA helped the effective separation of electrons-hole and improved the photocatalytic degradation rate. Our PTA/SCN is proposed as an environmental safety tool due to several advantages, such as low cost, convenient preparation, and efficient photocatalytic degradation of Rhodamine B.

Keywords: phosphotungstic acid, S-doped g-C_3N_4, photocatalytic degradation, Rhodamine B.

1. INTRODUCTION

With the development of society and the progress of technology, water environment pollution, has seriously threatened human life and health, especially the discharge of organic dyes in water [1]. Semiconductor photocatalysis technology has the advantages of low energy consumption, high efficiency, and good chemical stability (e.g., ZnO [2], TiO_2 [3], WO_3 [4], CdS [5], etc.), and is considered a green and low-cost technology for organic pollutant degradation [6, 7]. Carbon nitride (g-C_3N_4), an organic polymeric semiconductor material with a graphite-like structure, has the advantages of suitable forbidden band width (2.7 eV), non-toxicity, good chemical stability, and easy mass production, which has attracted much attention in photocatalytic degradation of organic pollutants [8 – 11]. However, g-C_3N_4 suffers from a high electron-hole complexation rate, low photoavailability, and small specific surface area, which limit its further application in the field of photocatalytic degradation of organic dyes [12 – 14]. Therefore, the non-metal/metal doping method, shape modulation, and construction of heterojunctions can improve the performance of g-C_3N_4 for photocatalytic degradation of organic dyes [15, 16]. Among them, non-metallic S-doped g-C_3N_4, which can improve the electrical conductivity and reduce the electron-hole complexation chance, and thus improve the photocatalytic degradation performance, has received a lot of attention [17 – 20].

Phosphotungstic acid (PTA) is the most acidic and electronegative solid acid with the highest outer oxygen atom among many heteropolyacids, and has been widely used in photocatalytic oxidation [21 – 23]. However, the small specific surface area and the small number of reactive sites of PTA limit the application of phosphotungstic acid in photocatalytic oxidation [24 – 27]. To overcome the shortcomings of phosphotungstic acid, it is generally solidly loaded onto suitable carriers to prepare composite photocatalysts, e.g., phosphotungstic acid solidly loaded onto TiO_2 significantly improves the degradation rate of aniline [28]; phosphotungstic acid solidly loaded onto g-C_3N_4 improves the photocatalytic degradation of rhodamine B [29]. There is no report on the application of phosphotungstic acid solid-loaded onto sulfur-doped g-C_3N_4 (SCN) in photocatalysis. Therefore, the fabrication of PTA and SCN heterojunction composites to further enhance the activity of photocatalytic degradation of rhodamine B (RhB) is of great significance.

In this paper, a series of PTA/SCN heterojunction composite photocatalysts were prepared by the reflux adsorption method using SCN prepared by the one-pot method as a carrier. The degradation performance of PTA/SCN heterojunction composite photocatalysts for RhB was investigated, and the photocatalytic degradation mechanism was explored.

2. EXPERIMENTAL

2.1. Materials and instruments

Thiourea (analytical pure, Maclean's Reagent Co., Ltd.), melamine (analytical pure, Maclean's Reagent Co., Ltd.), phosphotungstic acid (PTA, analytical pure, China Pharmaceutical Group), rhodamine B (analytical pure, China Pharmaceutical Group).

Xenon lamp (PLS-SXE300, Beijing Porphyry Technology Co., Ltd.), UV-Vis spectrophotometer (TUG1901, Beijing Pu-Analysis General Instrument Co., Ltd.), field emission scanning electron microscope (SEM) (JSMG 6700F, JEOL, Japan), X-ray diffractometer (XRD)

* Corresponding author. Tel.: +86-18883980584.
E-mail address: *jcxy20190119@cqcivc.edu.cn* (P. Li)

(X′PERT Pro, Philips, Netherlands), Fourier transform infrared spectrometer (FT-IR) (Nicolet 6700, Thermo Fisher Scientific Co., Ltd.).

2.2. Synthesis of SCN

The thioureas (5 g) were thoroughly ground in an agate mortar, then transferred to an alumina crucible, sealed with aluminum foil, placed in a Muffle furnace, and calcined at 550 ℃ (heating rate: 5 ℃/min^{-1}) for 3 hours. After cooling to room temperature naturally, light yellow powder SCN was obtained by grinding.

2.3. Synthesis of PTA/SCN photocatalysts

A series of PTA/SCN composites were prepared by the reflux adsorption method as described below. A certain amount of PTA was accurately weighed, dissolved in distilled water, and 0.4 g SCN was added with stirring. The reaction was stirred at 100 ℃ for 8 h. After the reaction, the solvent was evaporated at 70 ℃ and activated at 110 ℃ for 8 h to obtain x wt.% PTA/SCN composite photocatalytic materials (x = 5, 10, 20, 100), labeled as SCN5, SCN10, SCN20, SCN100, respectively.

2.4. Photocatalytic activity

Using RhB as the target organic dye for degradation, 0.01 g of PTA/SCN composite photocatalytic material was sonicated and dispersed in 100 mL of RhB solution (0.1 mg/mL) for 10 min in a dark reaction to reach the adsorption-resolution equilibrium. The solution was irradiated under a xenon lamp, and 10 ml was sampled every 10 min, centrifuged for 20 min (10000 rpm/min), and the absorbance of the solution was measured by UV-vis spectrophotometer at λ_{max} = 554 nm in the supernatant. The degradation rate of the photocatalytic degradation reaction was calculated from the change in absorbance before and after the solution with the formula:

$$\textit{Photocatalytic removal efficiency}\ (\%) = \frac{A_0 - A_t}{A_0} \times 100\%, \quad (1)$$

where A_0 is the absorbance at initial time t = 0 min, A_t is the absorbance of RhB solution after t min of illumination time.

3. RESULTS AND DISCUSSION

3.1. XRD analysis

The crystal structure of the photocatalytic material was characterized by XRD, and the results are shown in Fig. 1. The characteristic diffraction peaks of SCN in Fig. 1 are at 2θ = 13.2° and 27.5°, where the 13.2° corresponds to a crystallographic surface index of (100), which is characteristic of melon-like substances, and the 27.5° corresponds to a crystallographic surface index of (002), which is characteristic of interlayer stacking of aromatic substances. This indicates that SCN has a graphite-like structure [30]. The characteristic peak of SCN is slightly shifted towards a lower angle compared to the two characteristic peaks of pure g-C_3N_4, which may be related to the substitution of sulfur in the lattice atoms of carbon nitride [31]. In the XRD pattern of SCN20, it was observed that the intensity of the characteristic diffraction peak of melon analogues at 13.2° was weakened, mainly because PTA would react with the amino group of melon analogues in SCN, which in turn led to a decrease in the content of melon analogues [32]. Meanwhile, the characteristic diffraction peaks of PTA with a Keggin-type structure were observed at 10.4°, 21.4°, and 26.4°, which indicated that PTA still kept the Keggin-type structure after compounding with SCN and was uniformly solidly loaded onto SCN. With the increase of solid loading, the intensity of the diffraction peak corresponding to PTA did not show a significant enhancement, indicating that SCN played a good dispersing effect on PTA. In the XRD pattern of SCN20, the characteristic diffraction peak of SCN located at 27.5° is shifted to the right by about 1.2° (26.3°) after the solid loading of PTA, which is due to the disruption of the layer spacing of SCN by PTA, which in turn leads to an increase in the specific surface area.

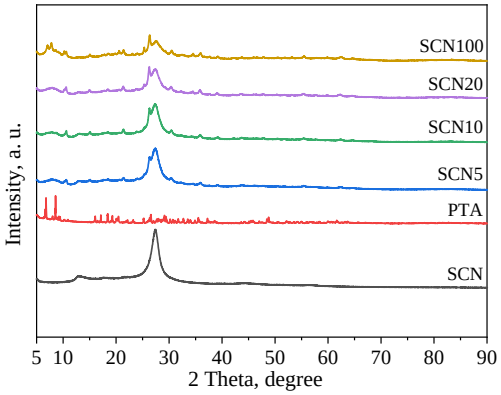

Fig. 1. XRD patterns of SCN, PTA, and serial PTA/SCN composites with different PTA content (SCN5, SCN10, SCN20, SCN100)

3.2. IR analysis

Fig. 2 shows the FT-IR spectra of SCN, PTA, SCN5, SCN10, SCN20, and SCN100.

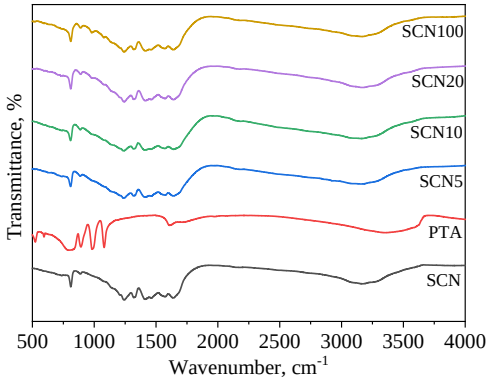

Fig. 2. FT-IR spectra of SCN, PTA, and serial PTA/SCN composites with different PTA content (SCN5, SCN10, SCN20, SCN100)

In the FT-IR spectra of pure PTA, the characteristic absorption peaks of PTA at 1083 cm^{-1}, 990 cm^{-1}, 893 cm^{-1}, and 805 cm^{-1} are attributed to the vibrational absorption of P-O, W-O, W-Ob-W, and W-Oc-W, respectively [32]. In the FT-IR spectrogram of SCN, the absorption peaks at 809 cm^{-1} and 889 cm^{-1} correspond to the C-N stretching vibrational characteristic absorption in the triazine ring,

and the absorption peaks at 1240 – 1650 cm^{-1} correspond to the stretching vibrational characteristic absorption of the carbon-nitrogen aromatic heterocyclic ring, and the broad band at 3100 – 3400 cm^{-1} corresponds to the stretching vibrational absorption of the N-H bond. The sulfur doping was revealed by the peak at 705 – cm^{-1}, which was attributed to the C-S stretching vibration [33, 34]. PTA/SCN photocatalytic materials, the intensity of the characteristic absorption peak at 3100 – 3400 cm^{-1} is weakened, which is attributed to the reaction of PTA with -NH_2 in SCN, resulting in the decrease of -NH_2 content in the PTA/SCN photocatalytic material, indicating that PTA and SCN are well compounded together in the form of chemical bonding [35].

3.3. SEM analysis

Scanning electron micrographs (SEM) of SCN, PTA, SCN5, SCN10, SCN20, and SCN100 photocatalytic materials, as shown in Fig. 3. Fig. 3 b shows that the PTA is an obvious block structure with uneven size, and after the solid loading of PTA (Fig. 3 c – f), no obvious PTA agglomeration is found, indicating that the PTA has been uniformly dispersed onto the SCN. Fig. 3 a shows that the SCN exhibits a blocky stacking structure, and after PTA solid loading (Fig. 3 c), the SCN still has some blocky structure, which is caused by the low solid loading of PTA. With the increase of PTA solid loading (Fig. 3 d – f), SCN showed a more obvious loose structure, indicating that PTA was homogenously dispersed on SCN. Thus, overall characterization techniques (XRD, FT-IR and TEM) used in this study successfully confirm the presence of S in the framework of g-C_3N_4 and that PTA and SCN are well compounded together in the form of a chemical bond.

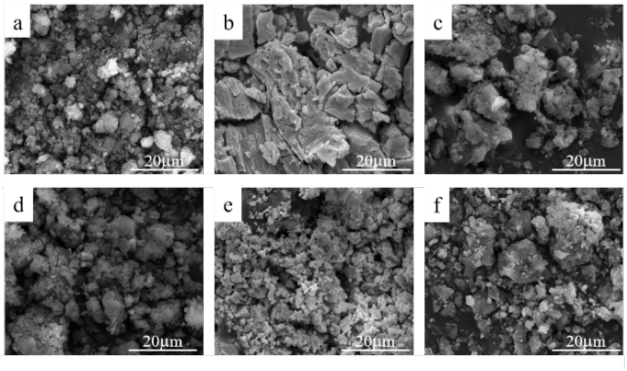

Fig. 3. SEM images: a – SCN; b – PTA; c – SCN5; d – SCN10; e – SCN20; f – SCN100

3.4. UV-Vis analysis

Fig. 4 shows the UV-Vis diffuse reflectance spectra of different photocatalytic materials. the absorption of SCN, PTA, SCN5, SCN10, SCN20, and SCN100 is mainly concentrated in the UV region and weakly absorbs visible light. As shown in Fig. 4, the absorption boundary of PTA is about 437 nm and that of SCN is about 486 nm [35]. Compared to PTA, the composite photocatalytic materials SCN5, SCN10, SCN20, and SCN100 not only increase the light absorption intensity but also red-shift the absorption boundary after solid loading of PTA. This is mainly due to the increase in specific surface area and the doping of SCN, which both increase the light absorption intensity [36].

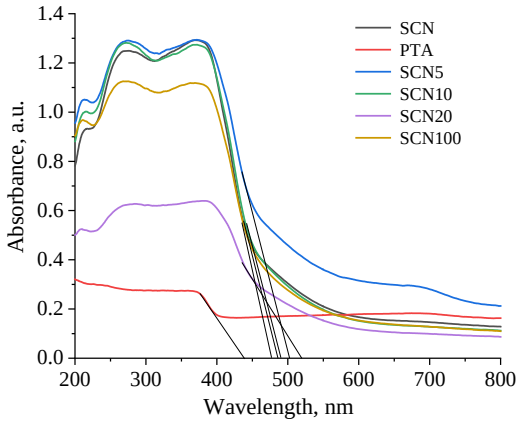

Fig. 4. UV-vis DRS spectra of SCN, PTA, and serial PTA/SCN composites with different PTA content (SCN5, SCN10, SCN20, SCN100)

The results of calculating the forbidden band gap (*Eg*) of the photocatalytic material using the equation: E*g* = 1239.9/g, *Eg* denotes the forbidden band gap width and *g* denotes the absorption boundary, are shown in Table 1 [19]. Compared with SCN, the forbidden band gap of SCN5 and SCN10 did not change significantly. The forbidden band width of SCN20 was the smallest, down to 2.39 eV. A smaller forbidden band gap allows for a red-shift in the absorption wavelength, which results in better absorption of visible light, generating more photogenerated electrons and improving photocatalytic efficiency [37].

Table 1. The band gap of photocatalysts

Photocatalytic materials	*g*, nm	*Eg*, eV
SCN	486	2.55
PTA	437	2.84
SCN5	502	2.47
SCN10	490	2.53
SCN20	519	2.39
SCN100	477	2.60

3.5. Photocatalytic activity

The photocatalytic activities of SCN5, SCN10, SCN20 and SCN100 for the degradation of RhB were investigated under the irradiation of a 300 W xenon lamp, and the results are shown in Fig. 5. After 60 min of light irradiation, the degradation rates of RhB were SCN20 (74 %), SCN100 (61 %), SCN10 (51 %) and SCN5 (34 %), respectively. The photocatalytic activity of PTA/SCN composite photocatalytic material for the photocatalytic degradation of RhB was much higher than that of PTA (39 %) and SCN (21 %). The results indicated that SCN20 had the highest photocatalytic activity, which was mainly due to the synergistic catalytic effect between SCN and PTA, and the doping of PTA and the increase in specific surface area resulted in more active sites on the surface of the catalyst. These results suggest that SCN20 is suitable for purifying wastewaters contaminated by dyes.

To further confirm the excellent photocatalytic performance of PTA/SCN, the photocatalytic activities of several SCN-based photocatalysts were summarized in Table 2. Interestingly, although the photocatalytic

degradation activity of SCN20 was not outstanding compared with the results listed in Table 2. But SCN20 still showed exciting demanding reaction conditions (i.e., high RhB amount (100 mg/L), and short reaction time (60 min)).

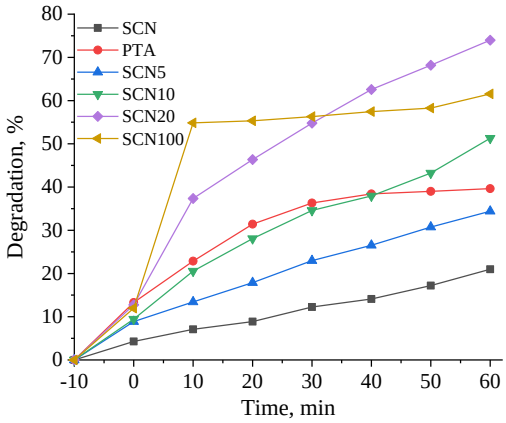

Fig. 5. Photocatalytic degradation RhB of different composites

The experimental data for the degradation of RhB by photocatalytic materials were fitted using the first order kinetic equation and the results are shown in Table 3. From Table 3, it can be seen that all photocatalytic materials degraded RhB following the first order kinetic equation [29]. Compared with SCN, the photocatalytic degradation rate of RhB degraded by the photocatalytic material SCN20 was 5 times higher, indicating that the photocatalytic degradation performance of the composites was significantly improved.

For catalysts, in addition to high catalytic activity, recyclability is also important. The recyclability of PTA/SCN complexes has been investigated. Fig. 6 shows the photocatalytic activity of the PTA/SCN complex after 5 cycles. From the graph, we can see that the degradation rate decreases as the recycling number increases, which can be attributed to the loss of catalyst during the recycling process.

3.6. Photocatalytic degradation mechanism

RhB was selected as the degrading organic pollutant and the photocatalytic degradation mechanism of SCN20 was investigated by free radical trapping experiments. P-benzoquinone (BQ), isopropyl alcohol (IPA), and disodium ethylenediaminetetraacetate (EDTA-2Na) were used as $\cdot O_2^-$, $\cdot OH$, and h_{VB}^+ trapping agents, respectively, and were added (1 mol/mL) before light exposure for 60 min. The results are shown in Fig. 7.

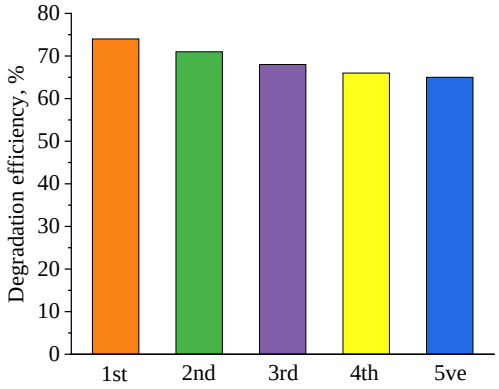

Fig. 6. The cyclic experiment of RhB degradation of SCN20 catalyst

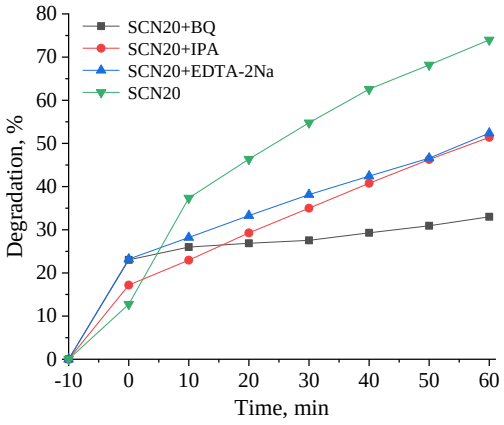

Fig. 7. Influence of different scavengers on the catalytic activity of SCN20

The results showed that the catalytic degradation rate decreased significantly when BQ was added, implying that $\cdot O_2^-$ was the main active species in the photocatalytic degradation reaction.

Table 2. Comparison of photoactivity of different SCN-based photocatalysts

Photocatalyst	Pollutant	Concentration	Degradation time	Efficiency	References
SCN/TiO_2	Congo Red	50 mg/L	60 min	97 %	[38]
SCN nanosheets	Methyl orange	10 mg/L	4 h	83 %	[39]
SCN nanosheets	Methylene blue	10 mg/L	3 h	97 %	[40]
SCN/SiO_2	Methyl orange	10 mg/L	210 min	83 %	[41]
SCN/ZnO	Ciprofloxacin	20 mg/L	210 min	98 %	[42]
SCN/ZnO	Rhodamine B	10 mg/L	80 min	98 %	[43]
SCN/CdS	Rhodamine B	10 mg/L	75 min	100 %	[44]
SCN/C_3N_4	Rhodamine B	10 mg/L	120 min	95 %	[45]

Table 3. Photocatalytic degradation rate constants (k) of RhB by photocatalysts

Photocatalytic materials	SCN	PTA	SCN5	SCN10	SCN20	SCN100
K(min^{-1}) $\times 10^{-3}$	1.60	2.30	2.78	4.58	8.79	1.48
R^2	0.979	0.968	0.998	0.976	0.998	0.860

Table 4. Effect of scavengers on the degradation of RhB by SCN20

Trapping agents	No	BQ	IPA	EDTA-2Na
R%	74	33	51	52

Meanwhile, the addition of EDTA-2Na and IPA also reduced the degradation rate of RhB, indicating that h_{VB}^+ and ·OH also played a dominant role in the photocatalytic degradation of RhB.

Based on these results, a possible mechanism for the photocatalytic degradation of RhB by SCN20 is proposed, as shown in Fig. 8. Under visible light irradiation, electrons (e^-) from SCN migrate from the valence band (VB) to the conduction band (CB), leaving a hole (h_{VB}^+) on the VB. At the same time, the photogenerated electrons generated on the CB can be further transferred to the surface and react with O_2 to produce superoxide radicals ($\cdot O_2^-$), which in turn react with RhB to degrade it into small molecules. The vacancies left in the VB can react with water to produce hydroxyl radicals (·OH), which can directly oxidise RhB to small molecules. As the CB of SCN is more negative than that of PTA, and the VB of PTA is more positive than that of SCN [46, 47], photogenerated electrons will migrate from the CB of SCN to the CB of PTA, while the holes stay in the VB of SCN, achieving an effective electron-hole separation and improving the photocatalytic degradation rate.

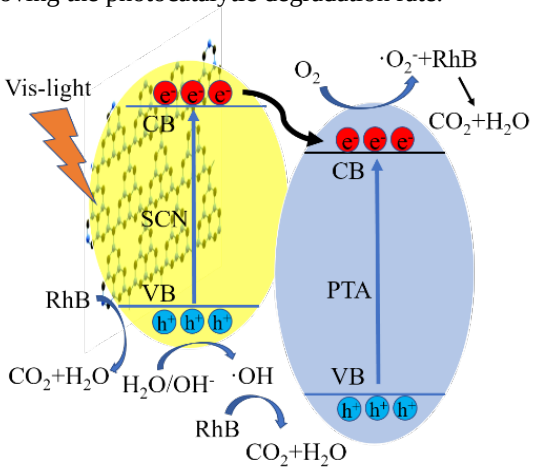

Fig. 8. A schematic illustration of the RhB degradation over PTA/SCN composite under visible light irradiation

4. CONCLUSIONS

A series of PTA/SCN composite photocatalytic materials were successfully prepared by a simple impregnation method using sulphur-doped g-C_3N_4 (SCN) prepared by the one-pot method as a carrier.XRD, FT-IR, SEM and UV-Vis showed that PTA was homogeneously dispersed in SCN and solidly loaded in SCN by chemical bonding; the forbidden band gap of the PTA/SCN composite photocatalytic materials became smaller and The PTA/SCN composite photocatalytic material has a smaller band gap, which reduces the electron-hole complexation rate and enhances the absorption of visible light. The photocatalytic degradation of RhB showed that different amounts of PTA had a significant effect on the photocatalytic degradation rate. Among them, SCN20 showed the highest photocatalytic degradation rate, which was 1.9 and 3.5 times higher than that of PTA and SCN respectively. This is because the solid loading of PTA, which disrupts the layer spacing of SCN, significantly affects the forbidden band gap of the composites, which in turn increases the photocatalytic degradation rate. The main active species in the photocatalytic degradation of the RhB system is $\cdot O_2^-$, while h_{VB}^+ and ·OH also played a dominant role in the photocatalytic degradation of RhB. Conclusively, PTA/SCN photocatalytic composites showed numerous advantages, such as inexpensive, easy preparation, and efficient degradation of dye. These characteristics allow PTA/SCN to be a candidate for photocatalytic degradation of printing and dyeing wastewater.

Acknowledgments

This work was financially supported partially by the Natural Science Foundation of Chongqing, China (grant No. cstc2021jcyj-msxmX0242).

REFERENCES

1. **Martínez-Huitle, C.A., Rodrigo, M.A., Sirés, I., Scialdone, O.** Single and Coupled Electrochemical Processes and Reactors for the Abatement of Organic Water Pollutants: A Critical Review *Chemical Reviews* 115 (24) 2015: pp. 13362 – 13407. https://doi.org/10.1021/acs.chemrev.5b00361
2. **Zhu, D., Zhou, Q.** Action and Mechanism of Semiconductor Photocatalysis on Degradation of Organic Pollutants in Water Treatment: A review *Environmental Nanotechnology Monitoring & Management* 12 2019: pp. 100255 – 100265. https://doi.org/10.1016/j.enmm.2019.100255
3. **Schneider, J., Matsuoka, M., Takeuchi, M., Zhang, J., Horiuchi, Y., Anpo, M., Bahnemann, M.D.** Understanding TiO_2 Photocatalysis: Mechanisms and Materials *Chemical Reviews* 114 (19) 2014: pp. 9919 – 9986. https://doi.org/10.1021/cr5001892
4. **Ayodhya, D., Veerabhadram, G.** A Review on Recent Advances in Photodegradation of Dyes Using Doped and Heterojunction Based Semiconductor Metal Sulfide Nanostructures for Environmental Protection *Materials Today Energy* 9 2018: pp. 83 – 113. https://doi.org/10.1016/j.mtener.2018.05.007
5. **He, F., Wang, Z., Li, Y., Peng, S., Liu, B.** The Nonmetal Modulation of Composition and Morphology of g-C3N4-Based Photocatalysts *Applied Catalysis B: Environmental* 269 (15) 2020: pp. 118828 – 118849. https://doi.org/10.1016/j.apcatb.2020.118828
6. **Liu, Z., Wang, G., Chen, H., Yang, P.** An Amorphous/crystalline g-C_3N_4 Homojunction for Visible Light Photocatalysis Reactions with Superior Activity *Chemical Communications* 54 2018: pp. 4720 – 4723. https://doi.org/10.1039/C8CC01824C
7. **Li, Y., Zhou, M., Cheng, B., Shao, Y.** Recent Advances in g-C_3N_4-based Heterojunction Photocatalysts *Journal of Materials Science and Technology* 56 (1) 2020: pp. 1 – 17. https://doi.org/10.1016/j.jmst.2020.04.028
8. **Yang, L., Liu, X., Liu, Z., Wang, C., Liu, G., Li, Q., Feng, X.** Enhanced Photocatalytic Activity of g-C_3N_4 2D Nanosheets Through Thermal Exfoliation Using

Dicyandiamide as Precursor *Ceramics International* 44 (17) 2018: pp. 20613 – 20619. https://doi.org/10.1016/j.ceramint.2018.06.105

9. **Nemiwal, M., Zhang, T.C., Kumar, D.** Recent Progress in g-C_3N_4, TiO_2 and ZnO Based Photocatalysts for Dye Degradation: Strategies to Improve Photocatalytic Activity *Science of The Total Environment* 767 2021: pp. 144896 – 144912. https://doi.org/10.1016/j.scitotenv.2020.144896
10. **Chang, F., Yan, W., Cheng, W., Wu, F., Hu, X.** The Construction and Enhanced Photocatalytic Performance of Binary Composite S/g-C_3N_4 *Materials Science in Semiconductor Processing* 87 2018: pp. 1 – 6. https://doi.org/10.1016/j.mssp.2018.07.005
11. **Liu, S., Zhu, H., Yao, W., Chen, K., Chen, D.** One Step Synthesis of P-doped g-C_3N_4 with the Enhanced Visible Light Photocatalytic Activity *Applied Surface Science* 430 2018: pp. 309 – 315. https://doi.org/10.1016/j.apsusc.2017.07.108
12. **Zhou, Y., Zhang, L., Huang, W., Kong, Q., Fan, X., Wang, M.** N-doped Graphitic Carbon-incorporated g-C_3N_4 for Remarkably Enhanced Photocatalytic H_2 Evolution under Visible Light *Carbon* 99 2016: pp. 111 – 117. https://doi.org/10.1016/j.carbon.2015.12.008
13. **Patnaik, S., Sahoo, D.P., Parida, K.** Recent Advances in Anion Doped g-C_3N_4 Photocatalysts: A review *Carbon* 172 2021: pp. 682 – 711. https://doi.org/10.1016/j.carbon.2020.10.073
14. **Li, Y., Xing, X., Pei, J., Li, R., Wen, Y., Cui, S. Liu, T.** Automobile Exhaust Gas Purification Material Based on Physical Adsorption of Tourmaline Powder and Visible Light Catalytic Decomposition of g-C_3N_4/$BiVO_4$ *Ceramics International* 46 (8) 2020: pp. 12637 – 12647. https://doi.org/10.1016/j.ceramint.2020.02.029
15. **Periyathambi, K., Hossain, M.S., Macadangdang, R.R., Madhubala, V., Palanivel, B., Venkatachalam, M., Massoud, E.S., Sreedevi, G.** ZnO Coupled F-doped g-C_3N_4: Z-scheme Heterojunction for Visible-light Driven Photocatalytic Degradation Reaction *Inorganic Chemistry Communications* 135 2022: pp. 109102 – 109109. https://doi.org/10.1016/j.inoche.2021.109102
16. **Sun, Q., Sun, Y., Zhou, M., Cheng, H., Chen, H., Dorus, B., Lu, M., Le, T.** A 2D/3D g-C_3N_4/ZnO Heterojunction Enhanced Visible-light Driven Photocatalytic Activity for Sulfonamides Degradation *Ceramics International* 48 2022: pp. 7283 – 7290. https://doi.org/10.1016/j.ceramint.2021.11.289
17. **Jeyaraman, A., Ramachandran, R., Chen, S.M., Karthik, R., Kumar, J.V., Shim, J., Shafi, M., Lee, J.** Raspberry-like $CuWO_4$ Hollow Spheres Anchored on Sulfur-doped g-C_3N_4 Composite: An Efficient Electrocatalyst for Selective Electrochemical Detection of Antibiotic Drug Nitrofurazone *Chemosphere* 296 2022: pp. 133997 – 134006. https://doi.org/10.1016/j.chemosphere.2022.133997
18. **Kang, L., Han, Z., Yu, H., Wu, Q., Yang, H.** Experimental and Theoretical Investigations on the Enhanced Photocatalytic Performance of Titanate Nanosheets/sulfur-Doped g-C_3N_4 Heterojunction: Synergistic Effects and Mechanistic Studies *Separation and Purification Technology* 278 2021: pp. 119482 – 119494. https://doi.org/10.1016/j.seppur.2021.119482
19. **Jiang, J., Xiong, Z., Wang, H., Liao, G., Bai, S., Zou, J., Wu, P., Zhang, P., Li, X.** Sulfur-doped g-C_3N_4/g-C_3N_4 Isotype Step-scheme Heterojunction for Photocatalytic H_2 Evolution *Journal of Materials Science & Technology* 118 2022: pp. 15 – 24. https://doi.org/10.1016/j.jmst.2021.12.018
20. **Gu, Y., Bao, A., Zhang, X., Yan, J., Du, Q., Zhang, M., Qi, X.** Facile Fabrication of Sulfur-doped Cu_2O and g-C_3N_4 with Z-scheme Structure for Enhanced Photocatalytic Water Splitting Performance *Materials Chemistry and Physics* 266 2021: pp. 124542 – 124549. https://doi.org/10.1016/j.matchemphys.2021.124542
21. **Ahmad, E., Pant, K.K., Haider, M.A.** Synthesis and Application of TiO_2-supported Phosphotungstic Acid for Ethyl Levulinate Production *Materials Science for Energy Technologies* 5 2022: pp. 189 – 196. https://doi.org/10.1016/j.mset.2022.02.001
22. **Zhu, W.** Phosphotungstic Acid Passivated Enhanced Photocatalytic Performance of ZnS Nanoparticles Under Solar Light *Solid State Sciences* 118 2021: pp. 106406 – 106415. https://doi.org/10.1016/j.solidstatesciences.2020.106406
23. **Khudhair, E.M., Ammar, S.H., Khadim, H.J.** Phosphotungstic Acid Immobilized onto ZnO Coated Zerovalent Iron (Fe@ZnO/PW) Core/shell Magnetic Nanocomposite for Enhanced Photocatalytic Bacterial Inactivation under Visible Light *Journal of Photochemistry and Photobiology A: Chemistry* 404 2021: pp. 112907 – 112918. https://doi.org/10.1016/j.jphotochem.2020.112907
24. **Li, H., Zhao, Y., Yin, C., Jiao, L., Ding, L.** WO_3 Nanocrystal Prepared by Self-assembly of Phosphotungstic Acid and Dopamine for Photocatalytic Degradation of Congo Red *Colloids and Surfaces A: Physicochemical and Engineering Aspects* 572 2019: pp. 147 – 151. https://doi.org/10.1016/j.colsurfa.2019.03.092
25. **Jiang, X., Zhang, Z., Sun, M., Liu, W., Huang, J., Xu, H.** Self-assembly of Highly-dispersed Phosphotungstic Acid Clusters onto Graphitic Carbon Nitride Nanosheets as Fascinating Molecular-scale Z-scheme Heterojunctions for Photocatalytic Solar-to-fuels Conversion *Applied Catalysis B: Environmental* 281 2021: pp. 119473 – 119487. https://doi.org/10.1016/j.apcatb.2020.119473
26. **Meng, P., Heng, H., Sun, Y., Huang, J., Yang, J., Liu, X.** Positive Effects of Phosphotungstic Acid on the In-situ Solid-state Polymerization and Visible Light Photocatalytic Activity of Polyimide-based Photocatalyst *Applied Catalysis B: Environmental* 226 2018: pp. 487 – 498. https://doi.org/10.1016/j.apcatb.2018.01.004
27. **Wang, S., Zhang, M., Feng, J., Wei, T., Ren, Y., Ma, J.** In-situ Polymerization of Polyaniline Modified by Phosphotungstic Acid on the Surface of Hollow Carbon for Two-way Efficient Reduction of Nitrate in Water *Chemical Engineering Journal* 430 (4) 2022: pp. 133175 – 133188. https://doi.org/10.1016/j.cej.2021.133175
28. **Taghavi, M., Ehrampoush, M.H., Ghaneian, M.T., Tabatabaee, M., Fakhri, Y.** Application of a Keggin-type Heteropoly Acid on Supporting Nanoparticles in Photocatalytic Degradation of Organic Pollutants in Aqueous Solutions *Journal of Cleaner Production* 179 (1) 2018: pp. 1447 – 1453. https://doi.org/10.1016/j.jclepro.2018.06.280
29. **Jie, Z., Cai, T., Li, H., Zhao, H.** Preparation of High Specific Surface Area g-C_3N_4 Doping by Phosphotungstic Acid and Its Photocatalytic Properties *Journal of Synthetic Crystals* 48 (1) 2019: pp. 101 – 109. https://doi.org/10.3969/j.issn.1000-985X.2019.01.017

30. **Tanga, L., Feng, C., Deng, Y., Zeng, G., Wang, J., Liu, Y., Feng, H., Wang, J.** Enhanced Photocatalytic Activity of Ternary Ag/g-C_3N_4/$NaTaO_3$ Photocatalysts Under Wide Spectrum Light Radiation: The High Potential Band Protection Mechanism *Applied Catalysis B Environmental* 230 2018: pp. 102 – 114. https://doi.org/10.1016/j.apcatb.2018.02.031

31. **Yang, S., Gong, Y., Zhang, J., Zhan, L., Ma, L., Fang, Z., Vajtai, R., Wang, X., Ajayan, P.M.** Exfoliated Graphitic Carbon Nitride Nanosheets as Efficient Catalysts for Hydrogen Evolution under Visible Light *Advanced Materials* 25 2013: pp. 2452 – 2456. https://doi.org/10.1002/chin.201331210

32. **Sampurnam, S., Muthamizh, S., Dhanasekaran, T., Latha, D., Padmanaban, A., Selvam, P., Stephen, A., Narayanan, V.** Synthesis and Characterization of Keggin-Type Polyoxometalate/zirconia Nanocomposites-comparison of its Photocatalytic Activity Towards Various Organic Pollutants *Journal of Photochemistry and Photobiology A: Chemistry* 370 2019: pp. 26 – 40. https://doi.org/10.1016/j.jphotochem.2018.10.031

33. **Chen, X., Kuo, D.H., Lu, D.** Nanonization of g-C_3N_4 with the Assistance of Activated Carbon for Improved Visible Light Photocatalysis *RSC Advances* 6 2019: pp. 66814 – 66821. https://doi.org/10.1039/C6RA10357J

34. **Hong, L.X., Zheng-Xin, T., Xian-Zhou, Z.** Molecular Structure, IR Spectra of 2-mercaptobenzothiazole and 2-mercaptobenzoxazole by Density Functional Theory and Ab initio Hartree-Fock Calculations *Spectrochimica Acta, Part A* 74 2009: pp. 168 – 173. https://doi.org/10.1016/j.saa.2009.05.026

35. **Mozhde, Y., Hossein, E., Mahdi, K.N.** Decoration of g-C_3N_4 by Inorganic Cluster of Polyoxometalate Through Organic Linker Strategy for Enhancing Photoelectrocatalytic Performance under Visible Light *International Journal of Hydrogen Energy* 47 2022: pp. 3001 – 3012. https://doi.org/10.1016/j.ijhydene.2021.10.253

36. **Ping, N., Zhang, L., Gang, L., Cheng, H.** Graphene-like Carbon Nitride Nanosheets for Improved Photocatalytic Activities *Advanced Functional Materials* 22 2012: pp. 4763 – 4770. https://doi.org/10.1002/adfm.201200922

37. **Wang, S., Lu, Q., Yan, X., Yang, M., Ye, R., Du, D., Lin, Y.** "On-Off-On" Fluorescence Sensor Based on g-C_3N_4 Nanosheets for Selective and Sequential Detection of Ag^+ and S^{2-} *Talanta* 168 2017: pp. 168 – 173. https://doi.org/10.1016/j.talanta.2017.03.004

38. **Wang, J., Wang, G., Cheng, B., Yu, J., Fan, J.** Sulfur-Doped g-C_3N_4/TiO_2 S-scheme Heterojunction Photocatalyst for Congo Red Photodegradation *Chinese Journal of Catalysis* 42 (1) 2021: pp. 56 – 68. https://doi.org/10.1016/S1872-2067(20)63634-8

39. **Cao, S., Fan, B., Feng, Y., Chen, H., Jiang, F., Wang, X.** Sulfur-doped g-C_3N_4 Nanosheets with Carbon Vacancies: General Synthesis and Improved Activity for Simulated Solar-light Photocatalytic Nitrogen Fixation *Chemical Engineering Journal* 353 2018: pp. 147 – 156. https://doi.org/10.1016/j.cej.2018.07.116

40. **Kadam, A.N., Moniruzzaman, M., Lee, S.W.** Dual Functional S-Doped g-C_3N_4 Pinhole Porous Nanosheets for Selective Fluorescence Sensing of Ag^+ and Visible-Light Photocatalysis of Dyes *Molecules* 24 (3) 2019: pp. 450 – 466. https://doi.org/10.3390/molecules24030450

41. **Jourshabani, M., Shariatinia, Z., Badiei, A.** Controllable Synthesis of Mesoporous Sulfur-Doped Carbon Nitride Materials for Enhanced Visible Light Photocatalytic Degradation *Langmuir* 33 2017: pp. 7062 – 7078. https://doi.org/10.1021/acs.langmuir.7b01767

42. **Gupta, B., Gupta, A.K., Ghosal, P.S., Tiwary, C.S.** Photo-induced Degradation of Biotoxic Ciprofloxacin Using the Porous 3D Hybrid Architecture of an Atomically Thin Sulfur-doped g-C_3N_4/ZnO Nanosheet *Environmental Research* 183 2020: pp. 109154 – 109168. https://doi.org/10.1016/j.envres.2020.109154

43. **Kalisamy, P., Lallimathi, M., Suryamathi, M., Palanivel, B., Venkatachalam, M.** ZnO Embedded S-doped g-C_3N_4 Heterojunction: Mediator-free Z-scheme Mechanism for Enhanced Charge Separation and Photocatalytic Degradation *RSC Advances* 10 (47) 2020: pp. 28365 – 28375. https://doi.org/10.1039/D0RA04642F

44. **Wu, Y., Wang, H., Tu, W.G., Wu, S.Y., Liu, Y., Tan, Y.Z., Luo, H.J., Yuan, X.Z., Chew, J.W.** Petal-like CdS Nanostructures Coated with Exfoliated Sulfur-doped Carbon Nitride via Chemically Activated Chain Termination for Enhanced Visible-light–driven Photocatalytic Water Purification and H_2 Generation *Applied Catalysis B: Environmental* 229 2018: pp. 181 – 191. https://doi.org/10.1016/j.apcatb.2018.02.029

45. **Hu, S.Z., Ma, L., Li, F.Y., Fan, Z.P., Wang, Q., Bai, J., Kang, X.X., Wu, G.** Construction of g-C_3N_4/S-g-C_3N_4 Metal-Free Isotype Heterojunctions with an Enhanced Charge Driving Force and Their Photocatalytic Performance Under Anoxic Conditions *RSC Advances* 5 2015: pp. 90750 – 90756. https://doi.org/10.1039/C5RA15611D

46. **Chen, J., Hong, Z., Chen, Y., Lin, B., Gao, B.** One-step Synthesis of Sulfur-doped and Nitrogen-deficient g-C_3N_4 Photocatalyst for Enhanced Hydrogen Evolution Under Visible Light *Materials Letters* 145 2015: pp. 129 – 132. https://doi.org/10.1016/j.matlet.2015.01.073

47. **Omwoma, S., Gore, C.T., Ji, Y., Hu, C., Song, Y.F.** Environmentally Benign Polyoxometalate Materials *Coordination Chemistry Reviews* 286 2015: pp. 17 – 29. https://doi.org/10.1016/j.ccr.2014.11.013